Effective Rate Constants for the Surface Reaction between Solid Methanol and Deuterium Atoms at 10 K

Akihiro Nagaoka,† Naoki Watanabe,* and Akira Kouchi

Institute of Low Temperature Science, Hokkaido University, N19W8, Kita-ku, Sapporo, Hokkaido 060-0819, Japan

Received: December 28, 2006; In Final Form: February 15, 2007

The surface reactions of CH_3OH, CH_2DOH, and CHD_2OH with cold D atoms at 10 K were investigated using an atomic beam source and FTIR. Methyl-deuterated isotopologues CH_2DOH, CHD_2OH, and CD_3OH were produced by exposure of amorphous solid CH_3OH to D atoms at 10 K, and the pseudo-first-order rates for the reactions $CH_3OH + D \rightarrow CH_2OH + HD$, $CH_2DOH + D \rightarrow CHDOH + HD$, and $CHD_2OH + D \rightarrow CD_2OH + HD$ were estimated. The ratios of the reaction rates of the second and third reactions to the first reaction were 0.69 ± 0.11 and 0.52 ± 0.14, respectively. The difference in reaction rates is thought to be due to a secondary kinetic isotope effect on the H-abstraction reaction from the methyl side by D atoms.

1. Introduction

The surface chemistry of solids at low temperatures is of physical and chemical interest as it allows observation of the quantum mechanical tunneling effect and also plays an important role in the astrophysical environment.[1,2] At low temperatures, the de Broglie wavelength of a light particle such as a hydrogen atom becomes comparable to typical reaction barrier widths, and thus the reactions can proceed via the atom-tunneling effect. Since the temperature in the cold regions of space is as low as 10 K, the tunneling reaction of hydrogen (H) atoms becomes very efficient in these areas. For example, in interstellar molecular clouds, which typically have a temperature of 10 K, tunneling reactions of H atoms with carbon monoxide (CO) on solid surfaces are a key process in the formation of interstellar formaldehyde (H_2CO) and methanol (CH_3OH) molecules, which are precursors of more complex organic molecules.[3−7]

Surface reactions between the deuterium (D) atom and other molecules at low temperatures are of interest because the kinetic isotope effect helps us to obtain information such as reaction barrier heights and widths. For reactions of CO with H and D atoms on solid water surfaces, the difference in the reaction rate constants due to the kinetic isotope effect has been determined experimentally as $k_D/k_H \sim 0.1$ at 15 K, and the barrier height and width for the reaction are constrained.[8] From the astrochemical viewpoint, the surface reaction $CH_3OH + D$ is especially interesting because this reaction process on cold interstellar grain surfaces contributes greatly to deuterium fractionation in interstellar methanol.[9,10]

Although low-temperature reactions of solid CH_3OH with radicals such as CH_3 have been studied extensively,[11] information about its reactions with H/D atoms is limited. Hiraoka and co-workers performed an experiment involving exposure of solid CH_3OH to D atoms at 10 K and reported that CH_2DOH was the only product obtained after 300 min of exposure.[12] Recently, we performed a similar experiment at 10 K and observed efficient formation of CH_2DOH, CHD_2OH, and CD_3OH at D-exposure times as short as a few minutes.[9] The difference between these two sets of results is thought to be due to a large difference in the flux of the D atoms. The flux in our experiment was measured as approximately 1×10^{14} atoms cm^{-2} s^{-1}, while the other group did not measure the flux of D atoms in their experiment but deduced it to be $<10^{13}$ atoms cm^{-2} s^{-1} based on the literature. In this paper, we report further experimental results for the surface reactions of methanol (CH_3OH, CH_2DOH, CHD_2OH, CH_3OD, and CD_3OD) with D atoms on amorphous solid samples at 10 K.

2. Experimental Section

2.1. Experimental Setup. Experiments were performed using the ASURA (apparatus for surface reactions in astrophysics) system (Figure 1). The details of the ASURA system are described in a previous report.[7] Briefly, the system consists of a main chamber, an atomic source chamber, a Fourier transform infrared (FTIR) spectrometer (Spectrum One, Perkin-Elmer), and a quadrupole mass spectrometer (QMS) (M-400QA-M, Anelva).

At the center of the main chamber, a mirror-finished aluminum (Al) substrate (30 mm in diameter) is mounted on an oxygen-free copper (Cu) holder attached to the cold head of a He refrigerator (RDK-415, Sumitomo Heavy Industries). A solid sample was vapor-deposited on the substrate at 10 K through a capillary plate (J5022−09, Hamamatsu Photonics; deposition angle of 30° to the surface normal of the substrate). The sample liquids used were CH_3OH (99.8% purity, Kishida Chemical Co., Ltd.), CH_2DOH (98% purity, Isotec), CHD_2OH (98% purity, Isotec), CH_3OD (99.5% purity, Aldrich), and CD_3OD (99.95% purity, Acros). Before deposition, we conducted several freeze−thaw cycles to eliminate contaminating gases in the sample liquids. The thickness of all solid samples was 3 monolayer (ML), which was measured by FTIR (see section 2.3 for details). The deposition rate was approximately 0.18 monolayer min^{-1}. In this paper, ML represents the amount of molecules deposited, on the assumption that 1 monolayer = 1×10^{15} molecule cm^{-2}, because the solid samples were not crystalline but amorphous solids.[13]

After deposition, the sample (10 K) was exposed to cold D atoms. D atoms were generated by a microwave discharge of

* Corresponding author. E-mail: watanabe@lowtem.hokudai.ac.jp. Tel.: +81-11-706-5501. Fax: +81-11-706-7142.

† JSPS Research Fellow.

10.1021/jp068978r CCC: $37.00
Published on Web 03/30/2007

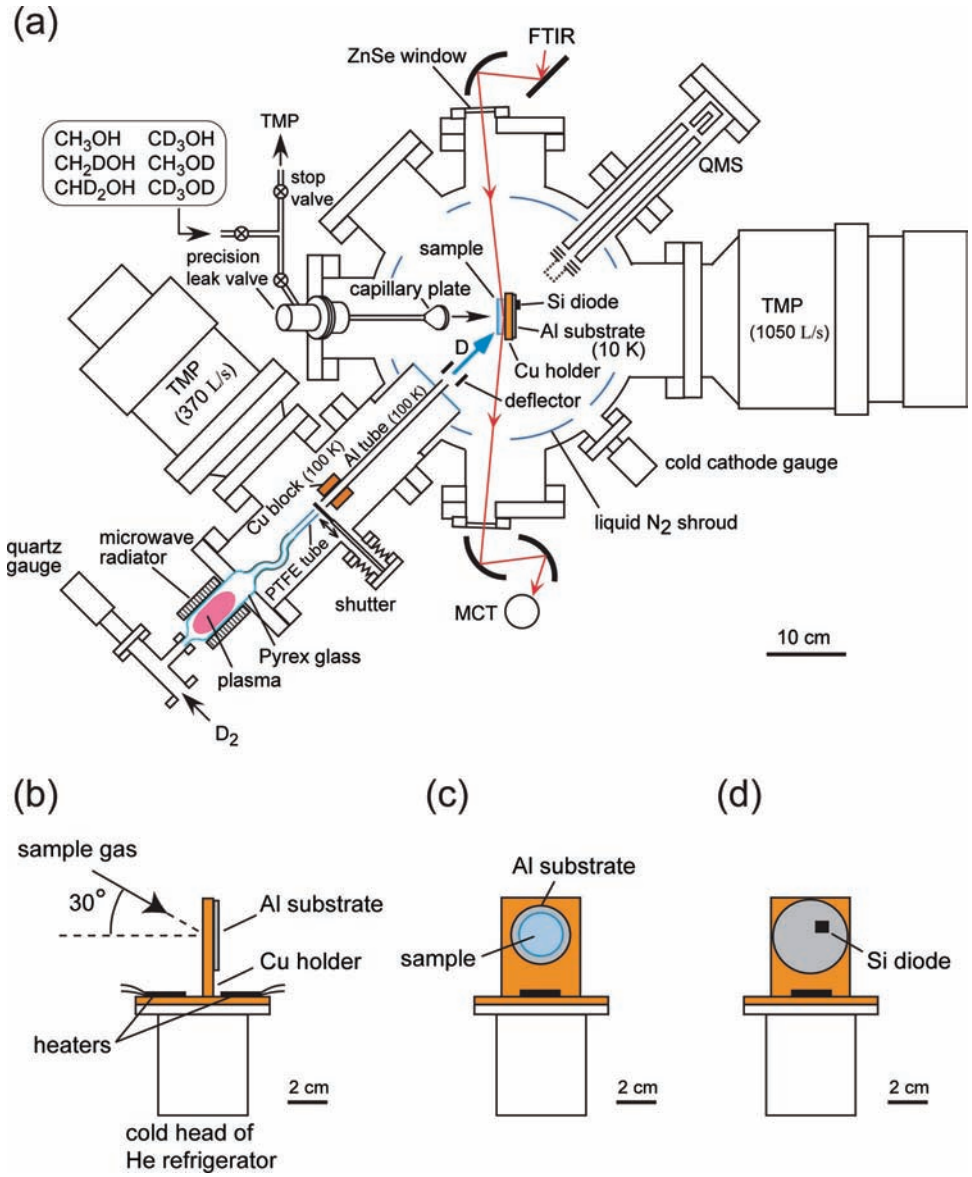

Figure 1. Schematic diagram of the ASURA system. (a) Top view. Side views of the substrate and the sample holder at the center of the main chamber from the (b) MCT side, (c) front side, and (d) back (TMP) side. The deposition angle of sample gases was 30° to the surface normal of the substrate.

D_2 (99.5% purity, Sumitomo Seika). D_2 gas of 0.3 Torr, measured using a quartz gauge (GC-210, Vacuum Products), was introduced into a Pyrex glass discharge tube after passing through a cold trap cooled with liquid nitrogen to eliminate contaminating gases. Microwaves of 2.45 GHz (MP-201, Arios) with a power of ~100 W was fed to a water-cooled copper radiator[14] surrounding the Pyrex glass discharge tube. Before exposure, D atoms were cooled to ~100 K by multiple collisions with the inner wall of a cold aluminum tube (Al: 99.70%) connected to a He refrigerator (V204SC5L, Daikin). The temperature of the Al tube can be measured using two Au/Fe 0.07% Chromel thermocouples attached to the vicinity of the refrigerator and the exit of the Al tube (see Figure 2) and is controllable from 20 to 300 K. In the present experiment, the tube temperature was set at 100 K. The flux of D atoms was measured by QMS using the same method as Hidaka et al.[8] and was approximately 1×10^{14} atoms cm^{-2} s^{-1}. Charged particles and metastable atoms which may be formed in the discharge tube can be eliminated by a deflector of 100 V cm^{-1} located at the exit of the Al tube. We used a photodiode (IRD AXUV-100G) to check whether UV photons from the D_2 plasma in the discharge tube reached the substrate, but no UV photons were detected.

The change in the chemical composition of the sample was measured using FTIR, in situ, with a resolution of 4 cm^{-1}. The incident angle of the IR beam was 83° to the surface normal of the substrate. The main chamber and the atomic source chamber were evacuated by turbomolecular pumps, TG-900M (Osaka Vacuum, 900 L/s for N_2 and 1050 L/s for H_2) and TURBOVAC-340M (Leybold, 400 L/s for N_2 and 370 L/s for H_2), and the base pressures were $3-4 \times 10^{-10}$ and $5-6 \times 10^{-9}$ Torr, respectively. The pressures during D atom exposure were $2-3 \times 10^{-7}$ and $8-9 \times 10^{-6}$ Torr for the main chamber and the atomic source chamber, respectively. The temperature of the Al substrate was measured using a Si-diode sensor (DT-470, Lakeshore, accuracy ± 0.2 K) and was controlled with two ceramic heaters (100 W) attached at the cold head of the He refrigerator.

2.2. Measurement of Translational Temperature of Hydrogen (Deuterium) Atoms. We used cold D atoms of ~100 K to simulate surface reactions on dust grains in cold interstellar clouds. To confirm the kinetic temperature of atoms and evaluate

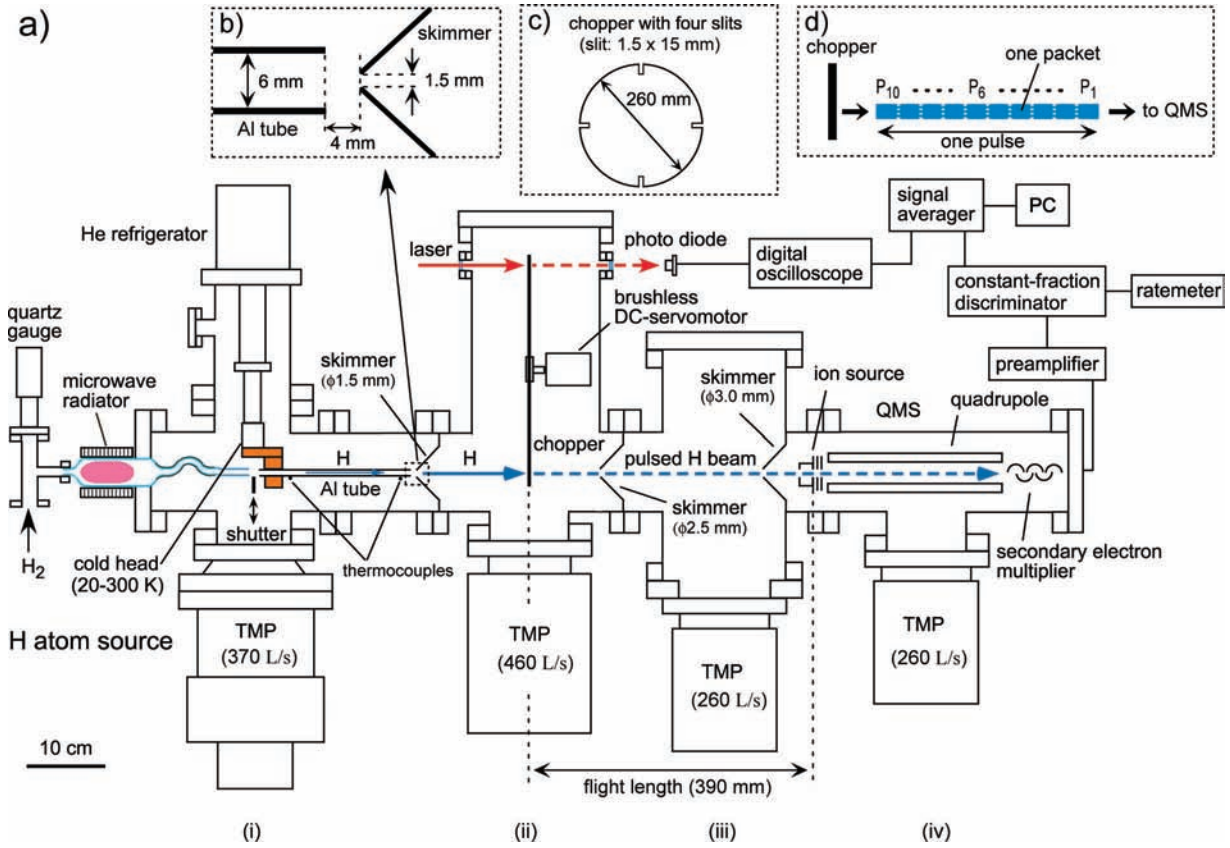

Figure 2. (a) Schematic diagram of the experimental system for TOF measurement (side view). The apparatus consists of (i) atomic source chamber, (ii) chopping chamber, (iii) differential pumping chamber, (iv) QMS chamber, and signal processing system. (b) Close-up of the vicinity of the first skimmer. (c) Chopper disk. (d) Conceptual illustration of the H pulse beam. We regard one pulse as a series of 10 packets in analysis of the TOF spectrum (see section 2.2 for details).

the performance of our cooling system, we performed a time-of-flight (TOF) measurement for H atoms using the experimental system shown in Figure 2. The apparatus consists of a signal processing system and four vacuum chambers: (i) atomic source chamber, (ii) chopping chamber, (iii) differential pumping chamber, and (iv) QMS chamber. Three skimmers (ϕ 1.5, 2.5, and 3.0 mm) were mounted between the chambers. The chambers were differentially pumped using turbomolecular pumps: (i) TURBOVAC-340M, Leybold, 370 L/s for H_2; (ii) STP-451, Seiko Seiki, 460 L/s; and (iii), (iv) PT-300, Mitsubishi Heavy Industries, 260 L/s. Base pressures were (i) 7×10^{-8}, (ii) 5×10^{-8}, (iii) 5×10^{-9}, and (iv) 7×10^{-9} Torr. The pressures in the chambers during TOF measurement were (i) 5×10^{-5}, (ii) 7×10^{-7}, (iii) 6×10^{-9}, and (iv) 9×10^{-9} Torr when the source pressure of H_2 was 0.3 Torr.

The atomic H beam was collimated by the first skimmer (ϕ 1.5 mm) and pulsed in the chopping chamber by a four-slit disk chopper mounted on a brushless DC-servomotor (Faulhaber, 3564K048B-K179−K1155). The timing of H pulse formation was measured using a He−Ne laser and a photodiode. The flight time was started at the moment of detection of the laser pulse. The frequency of the pulse formation and the pulse width were 66.66 Hz and 100 μs, respectively. After ionization at the ion source of a QMS (AQA-360, Anelva), the H pulses reached a secondary electron multiplier (SEM). The pulse signals were integrated by a signal averager (ELK-5120AVE, Electronica). We defined the flight length as the distance between the disk chopper and the ion source. The TOF of H^+ from the ion source to the SEM was very short compared with that from the disk chopper and the ion source, because the H^+ formed in the ion source was accelerated with 3 V at the ion lens.

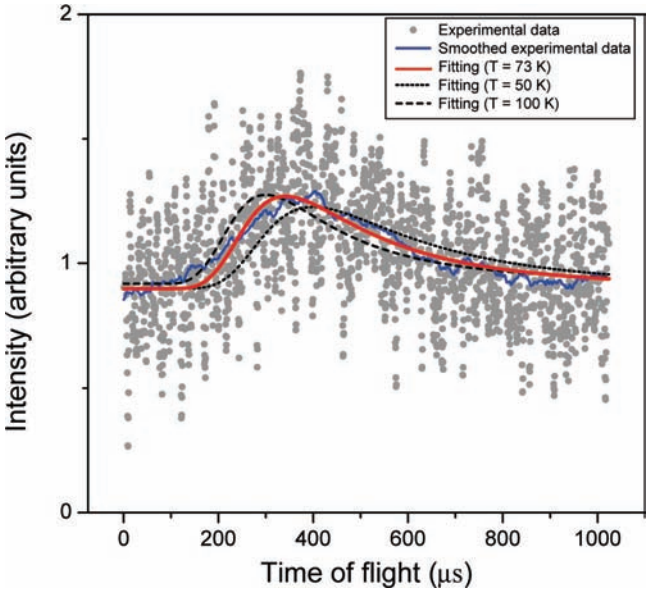

Figure 3. TOF spectrum of H atoms (Al tube: 50 K) and the fitting results by the least-square method using the modified Maxwell−Boltzmann transmission function (2). The blue continuous line represents the smoothed experimental data. The best-fitting result was at $T = 73$ K (red continuous), which clearly reproduces the experiment better than the fitted curves at $T = 50$ (black dotted) and 100 K (black dashed).

Figure 3 shows the TOF spectrum of H atoms. The velocity distribution function of gas molecules that have come through the skimmer is represented by the Maxwell−Boltzmann trans-

mission function:

$$f(v) = 4\pi\left(\frac{m}{2\pi k_B T}\right)^{3/2} v^3 \exp\left(-\frac{mv^2}{2k_B T}\right) \quad (1)$$

where v is the translational velocity of the gas molecule, m is the mass of the gas molecule, k_B is the Boltzmann constant, and T is the temperature. Under the present experimental conditions, eq 1 cannot be used directly for analysis of the TOF spectrum for H atoms, because the pulse width of 100 μs is comparable to the TOF of H ($\sim$270 μs at $T = 100$ K); that is, the TOF spectrum is broadened to a longer time because of the wide time span in one pulse. We therefore used a modified function that takes account of the time difference:

$$f(v) = A\sum_{n=0}^{9} 4\pi\left(\frac{m}{2\pi k_B T}\right)^{3/2}\left(\frac{l}{t-10n}\times 10^6\right)^3 \times \exp\left(-m\left(\frac{l}{t-10n}\times 10^6\right)^2 \frac{1}{2k_B T}\right) \quad (2)$$

where A is the proportional constant, t is the time (μs), and l is the flight length of 0.39 m. In eq 2, we regard one pulse as a series of 10 packets P_{n+1} ($n = 0-9$, see Figure 2d). The packet P_{n+1} has a delay of $10 \times n$ μs ($n = 0-9$) in its start time.

The fitting of the results by the least-square method using eq 2 for H atoms is shown in Figure 3. The best fit for the measured TOF spectrum was obtained at 73 K; hence, the H atoms are effectively cooled to near the tube temperature. We also measured the TOF of D atoms and H_2 and D_2 molecules at 50 K and obtained the same result as that for H. When the Al tube was set at 20 K, the intensity of the TOF signal for H was 1 order of magnitude smaller than that at 50 K. This indicates that approximately 90% of the H atoms stuck and recombined at the inner wall of the Al tube.

We also evaluated the performance of the previously used atom cooling system (see Figure 1 in Hidaka et al.[6]) using the TOF measurement system. In our past experiments, a polytetrafluoroethylene (PTFE) tube was used for atom cooling. The use of PTFE is known to suppress hydrogen atom recombination ($H + H \rightarrow H_2$) at the surface.[15] The PTFE tube was tightly covered with a copper tube which was connected to the cold head. The translational temperature of H through the PTFE tube was found to be approximately 200 K when the outer copper tube was at 30 K, indicating that this type of cooling tube does not work well. The reason for this may be the difference in the rates of thermal expansion of copper and PTFE. Since the rate of the thermal expansion of PTFE is approximately 1 order of magnitude greater than that of copper at 30 K,[16] thermal contact between the PTFE and the copper deteriorates at low temperatures, which means that the PTFE is not cooled to the temperature of the copper tube.

2.3. Infrared Spectra and Relative Integrated Band Strengths of Solid CH_3OH and Deuterated Isotopologues (CH_2DOH, CHD_2OH, CD_3OH, CH_3OD, and CD_3OD). To calculate the column densities of solid CH_3OH and its deuterated isotopologues, the integrated band strengths of these species are required. As these values have not yet been reported for the solid deuterated isotopologues, we measured the integrated band strengths of pure solid CH_2DOH, CH_3OD, CHD_2OH, CD_3OH, and CD_3OD relative to CH_3OH at 10 K using the ASURA system.

The solid samples were produced by vapor deposition of CH_3OH, CH_2DOH, CH_3OD, CHD_2OH, CD_3OH (99.5% purity, Acros), and CD_3OD through a capillary plate. To maintain a constant deposition rate during the experiments, the sample gas was turned on and off using a stop valve (SS-BNVCR4, Swagelok), and no adjustments were made to the precision leak valve (951−7172, Anelva). After the gas was turned off, the gas line was immediately evacuated. To avoid contamination, we measured one isotopologue per day.

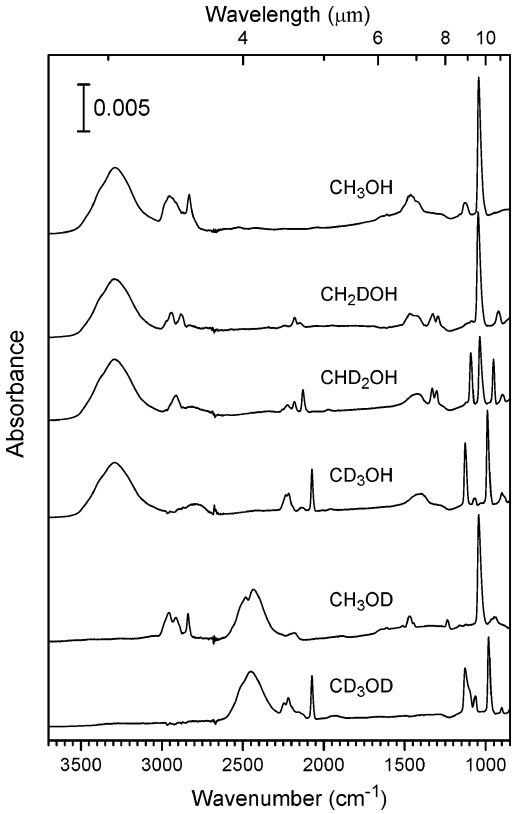

Figure 4. Infrared absorption spectra of amorphous solid CH_3OH, CH_2DOH, CH_3OD, CHD_2OH, CD_3OH, and CD_3OD deposited on the Al substrate at 10 K. Absorbance was obtained as common logarithms. The thickness of the samples is 3 monolayer. Spikes near 2675 cm^{-1} are noise caused by the vibration of the He refrigerator.

Figure 4 shows infrared absorption spectra of solid CH_3OH and isotopologues of 3 monolayer at 10 K. The shape of the −OH (−OD) stretching mode in the vicinity of 3300 (2450) cm^{-1} for the isotopologues indicates an amorphous structure in the samples.[13] The thickness of solid CH_3OH was estimated from the integrated area absorbance of the C−O stretching mode at 1043.6 cm^{-1} and the integrated band strength of 1.8×10^{-17} cm molecule^{-1}.[17,18] The deposition rate was approximately 0.6 monolayer min^{-1}.

To quantify the amount of molecules in the solid samples (thickness of the samples) before and after D exposure using integrated band strengths, the linearity between the thickness and the integrated area absorbance had to be checked. Figure 5 shows the relationship between deposition time/thickness and integrated area absorbance for solid CH_3OH at 10 K. The linearity between the deposition time and the integrated area absorbance was fairly good within the present experimental duration, which suggests that the sticking coefficients of CH_3OH molecules to the substrate and the solid CH_3OH surfaces are constant at least up to a deposition time of 20 min. We also estimated the thickness of the samples using the temperature-programmed desorption (TPD) method;[19] the results are consistent with those obtained using integrated band strengths. We thus conclude that the linearity between the integrated area absorbance and the sample thickness is good, and the relative

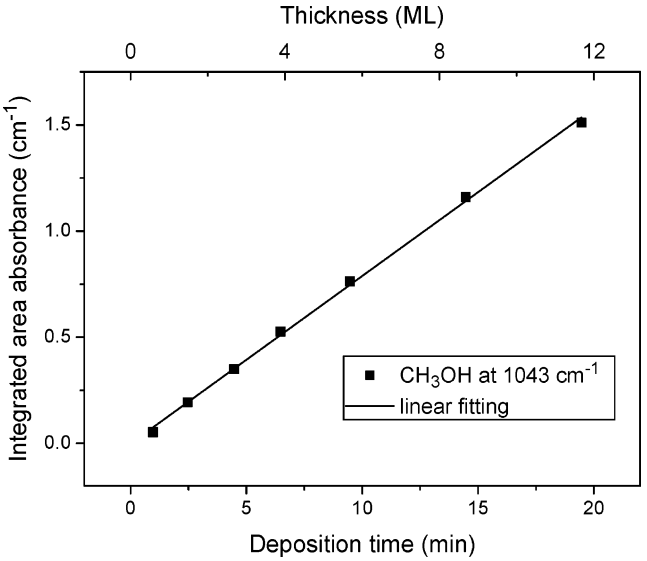

Figure 5. Increase in integrated area absorbance at 1043 cm^{-1} in the infrared spectra of amorphous solid CH_3OH at 10 K with deposition time. The upper abscissa represents the thickness of the solid CH_3OH samples estimated by the TPD method.[19] The solid line is the result of linear fitting.

integrated band strengths measured in the present work can be used for quantification. Similar measurements were also performed for all of the deuterated isotopologues listed above, and good linearity was confirmed. Hence, the relative integrated band strengths listed in Table 1 were obtained from the gradients of the linear fitted lines for all bands in the solid samples (e.g., see Figure 5).

3. Results and Discussion

3.1. Exposure of Amorphous Solid CH_3OH to D Atoms. Figure 6 shows the infrared absorption spectrum of amorphous solid CH_3OH and the change in the spectrum after exposure to cold D atoms at 10 K. As shown in Figure 6b, CH_2DOH, CHD_2OH, and CD_3OH appear with the consumption of CH_3OH. Isotopologues containing an −OD group, such as CH_3OD and CD_3OD, were not detected. Other molecules (e.g., H_2CO, HDCO, D_2CO, and CO) were also undetected. The detection limit of the ASURA system is $\sim 1 \times 10^{12}$ molecule cm^{-2} ($\sim$0.001 ML) for CH_3OH. After D atom exposure, we maintained the solid samples at 10 K for several hours, but no change was observed in the spectrum, suggesting that no additional slow reaction proceeds at 10 K after termination of exposure. Exposure of solid CH_3OH to D_2, HD, and H_2 molecules at 10 K did not induce any change in the spectrum. We performed a blank test[20] to check for contamination in the discharge tube and the Al tube, but no CH_3OH, deuterated isotopologues, or other molecules were detected; this is in agreement with results reported elsewhere.[3−10] This shows that both the discharge tube and the Al tube were uncontaminated by sample molecules; therefore, the obtained methanol isotopologues were produced via surface reactions with D atoms.

Figure 7 demonstrates the procedure for assignment of products and determination of molecular column densities. As can be seen in spectra a, b, and c in Figure 7, the bands at (ii) 920.8, (iv) 951.9, and (v) 988.4 cm^{-1} appear only for CH_2DOH, CHD_2OH, and CD_3OH, respectively. Therefore, these products are easily assigned and quantified in the exposed CH_3OH sample (spectrum d). In contrast, the decrease in CH_3OH should be carefully estimated because all of the CH_3OH bands overlap with those of the isotopologues. For example, the main band of CH_3OH is located at 1043.6 cm^{-1}, with the width of the base lying between 1000 and 1070 cm^{-1}, while CH_2DOH and CHD_2OH have bands at (i) 1046.9 cm^{-1} (base width 1005−1070 cm^{-1}) and (iii) 1036.7 cm^{-1} (base width 1000−1060 cm^{-1}), respectively; the dip (vi) at 1050 cm^{-1} in the spectrum of the exposed sample d consists of a decrease in the main band (CH_3OH) and an increase in product bands (i) and (iii) (CH_2DOH and CHD_2OH, respectively). Fortunately, we had obtained the integrated band strengths of bands (i) and (iii) relative to those of (ii) and (iv), respectively, as listed in Table 1. Therefore, in the spectrum of the exposed sample d, the contribution of bands (i) and (iii) in the dip (vi) can be estimated from the increase in bands (ii) and (iv).

Variations in the column densities of molecules in the sample (ΔN_t, molecule cm^{-2}) due to D atom exposure were calculated using the integrated band strengths shown in Table 1; these are plotted in Figure 8. ΔN_t is defined as $\Delta N(\mathrm{X})_t = N(\mathrm{X})_t - N(\mathrm{X})_{t=0}$ for molecule X, where $N(\mathrm{X})_t$ is the column density at an exposure time of t min. Since the spectra in Figure 6b were obtained by subtracting the initial ($t = 0$) spectrum (Figure 6a) from the spectra after t min exposure, ΔN_t values were calculated from the integrated area absorbance in the spectra shown in Figure 6b and these integrated band strengths using the following equations:

$$\Delta N(\mathrm{CH_3OH})_t = \alpha\left[\Delta A(1000-1070\ \mathrm{cm^{-1}})_t - \Delta A(920.8\ \mathrm{cm^{-1}})_t \times \frac{0.863}{0.105} - \Delta A(951.9\ \mathrm{cm^{-1}})_t \times \frac{0.432}{0.181}\right] \quad (3a)$$

$$\Delta N(\mathrm{CH_2DOH})_t = \frac{\alpha}{0.105} \times \Delta A(920.8\ \mathrm{cm^{-1}})_t \quad (3b)$$

$$\Delta N(\mathrm{CHD_2OH})_t = \frac{\alpha}{0.181} \times \Delta A(951.9\ \mathrm{cm^{-1}})_t \quad (3c)$$

$$\Delta N(\mathrm{CD_3OH})_t = \frac{\alpha}{0.484} \times \Delta A(988.4\ \mathrm{cm^{-1}})_t \quad (3d)$$

$$\alpha = \frac{\cos 83^\circ}{2\epsilon} \quad (3e)$$

where $\Delta A(\mathrm{X\ cm^{-1}})_t$ (cm^{-1}) is the integrated area absorbance at X cm^{-1} and ϵ (cm $molecule^{-1}$) is the integrated band strength of the C−O stretching mode in CH_3OH. Variations in the column density at the beginning of exposure ($t < 5$ min), as shown in Figure 8, indicate that CH_2DOH forms first, and subsequently CHD_2OH and CD_3OH appear, with the concurrent consumption of CH_3OH. In addition, CH_2DOH and CHD_2OH have maxima at approximately 5 and 20 min, respectively. These features strongly suggest that CH_2DOH, CHD_2OH, and CD_3OH are produced by the following successive H−D substitution reactions:

$$\mathrm{CH_3OH} \xrightarrow{k_1} \mathrm{CH_2DOH} \xrightarrow{k_2} \mathrm{CHD_2OH} \xrightarrow{k_3} \mathrm{CD_3OH} \quad (4)$$

where k_1, k_2, and k_3 are the reaction rate constants. If deuterated isotopologues were produced in parallel by reactions such as $CH_3OH \rightarrow CH_2DOH$, $CH_3OH \rightarrow CHD_2OH$, and $CH_3OH \rightarrow CD_3OH$, then CH_2DOH and CHD_2OH would not have maxima. The sum of the products ($CH_2DOH + CHD_2OH + CD_3OH$; diamonds in Figure 8) is very close to the amount by which CH_3OH decreased in the same exposure time, showing that desorption of CH_3OH and products during D exposure is

TABLE 1: Infrared Band Positions and Relative Integrated Band Strengths

molecule	band position[a] (cm^{-1})	assignment[b]	relative integrated band strength[c]	no. for Figure 7
CH_3OH	3397.4 ± 10.9[d]	OH stretching	1.068	
	3274.3 ± 2.9[d]	OH stretching	3.348	
	2987.6 ± 1.0[d]	CH_3 asym. stretching	0.053	
	2956.5 ± 4.0[d]	CH_3 asym. stretching or CH_3 sym. bending	0.476	
	2907.0 ± 4.8[d]	CH_3 asym. stretching or CH_3 asym. bending + CH_3 sym. bending	0.404	
	2862.6 ± 1.9[d]	CH_3 sym. stretching or sym. bending	0.073	
	2831.2 ± 0.2[d]	CH_3 sym. stretching	0.298	
	2821.3 ± 4.5[d]	CH_3 sym. stretching	0.139	
	2606.9 ± 1.7[d]	OH bending + CH_3 rocking	0.049	
	2530.2 ± 1.0[d]	OH bending + CH_3 rocking	0.062	
	2422.2 ± 1.6[d]	CH_3 rocking	0.088	
	2247.2 ± 2.9[d]	CH_3 rocking	0.016	
	2046.2 ± 1.4[d]	CO stretching	0.014	
	1491.4 ± 1.0[d]	CH_3 asym. bending	0.147	
	1477.4 ± 0.4[d]	CH_3 asym. bending or CH_3 sym. bending	0.051	
	1463.5 ± 0.3[d]	CH_3 asym. bending	0.035	
	1449.6 ± 0.5[d]	CH_3 sym. bending	0.070	
	1421.4 ± 0.3[d]	OH bending	0.170	
	1163.5 ± 1.4[d]	CH_3 rocking	0.007	
	1125.8 ± 0.2[d]	CH_3 rocking	0.142	
	1043.6 ± 0.1	CO stretching	1.000	
CH_2DOH	3418.8 ± 3.1[d]	OH stretching	0.263	
	3291.2 ± 3.2[d]	OH stretching	3.300	
	2977.3 ± 0.6[d]	CH_2 asym. stretching	0.046	
	2941.2 ± 0.3[d]	CH_2 asym.stretching	0.235	
	2905.1 ± 2.1[d]	CH_2 sym. stretching	0.020	
	2882.6 ± 0.2[d]	CH_2 sym. stretching	0.191	
	2818.9 ± 1.0[d]	CH_2 sym. stretching?	0.139	
	2725.2 ± 1.6[d]	?	0.058	
	2241.5 ± 0.2[d]	?	0.027	
	2180.2 ± 0.1[d]	CH_2 rocking	0.077	
	2147.2 ± 0.3[d]	CD stretching	0.041	
	1467.7 ± 0.4[d]	CH_2 bending	0.175	
	1419.1 ± 0.5[d]	OH bending?	0.129	
	1328.3 ± 0.1[d]	CH_2 twisting	0.119	
	1292.7 ± 0.1[d]	OH bending	0.058	
	1110.9 ± 6.0[d]	CH_2 rocking	0.043	
	1082.4 ± 1.9[d]	CH_2 rocking	0.033	
	1046.9 ± 0.1[d]	CO stretching	0.863	i
	920.8 ± 0.2	CD bending	0.105	ii
CHD_2OH	3420.9 ± 2.5[d]	OH stretching	0.352	
	3292.6 ± 3.1[d]	OH stretching	3.335	
	2977.3 ± 1.4[d]	CH stretching	0.012	
	2951.3 ± 0.8[d]	CO stretching	0.032	
	2915.5 ± 0.4[d]	CH stretching	0.255	
	2867.5 ± 1.0[d]	?	0.004	
	2815.9 ± 1.4[d]	?	0.403	
	2713.7 ± 1.3[d]	?	0.038	
	2256.0 ± 1.5[d]	CD_2 rocking	0.003	
	2224.8 ± 0.5[d]	CD_2 asym. stretching	0.073	
	2181.4 ± 0.2[d]	CD_2 bending	0.057	
	2128.4 ± 0.1	CD_2 sym. stretching	0.124	
	1973.0 ± 2.0	CO stretching + CD_2 wagging?	0.012	
	1448.4 ± 1.1[d]	OH bending?	0.222	
	1404.9 ± 0.3[d]	OH bending?	0.072	
	1330.4 ± 0.1[d]	CH bending	0.090	
	1303.4 ± 0.1[d]	CH bending	0.080	
	1120.6 ± 1.4[d]	CD_2 bending	0.016	
	1090.2 ± 0.1[d]	CD_2 bending	0.273	
	1036.7 ± 0.1	CO stretching	0.432	iii
	951.9 ± 0.1[d]	CD_2 wagging	0.181	iv
	898.3 ± 4.1[d]	CD_2 twisting	0.059	
	887.2 ± 2.3[d]	CD_2 twisting?	0.008	
CD_3OH	3421.3 ± 6.2[d]	OH stretching	0.341	
	3289.3 ± 2.1[d]	OH stretching	3.403	
	2802.1 ± 0.9[d]	OH bending	0.504	
	2246.1 ± 0.4[d]	CD_3 asym. stretching	0.072	
	2235.1 ± 0.1[d]	CD_3 asym. stretching	0.036	
	2215.7 ± 0.1[d]	CD_3 asym. stretching	0.130	
	2191.7 ± 0.1[d]	?	0.016	
	2146.1 ± 4.5[d]	CD_3 asym. bending	0.009	
	2129.7 ± 7.0[d]	CD_3 asym. bending	0.024	
	2093.5 ± 1.4[d]	CD_3 sym. stretching	0.003	

TABLE 1: (Continued)

molecule	band position[a] (cm^{-1})	assignment[b]	relative integrated band strength[c]	no. for Figure 7
CD_3OH (contd)	2073.0 ± 0.1[d]	CD_3 sym. stretching	0.172	
	2009.3 ± 3.0[d]	?	0.002	
	1957.1 ± 2.0[d]	CO stretching	0.011	
	1427.2 ± 0.4[d]	OH bending	0.274	
	1384.1 ± 0.2[d]	OH bending	0.056	
	1126.4 ± 0.1	CD_3 sym. bending	0.328	
	1068.0 ± 0.5	CD_3 asym. bending	0.036	
	1030.1 ± 1.0	CD_3 asym. bending	0.003	
	988.4 ± 0.1	CO stretching	0.484	v
	916.6 ± 5.4[d]	CD_3 rocking	0.011	
	899.9 ± 0.6[d]	CD_3 rocking	0.052	
	883.0 ± 1.0[d]	CD_3 rocking	0.028	
CH_3OD	2985.6 ± 1.6[d]	CH_3 asym. stretching	0.095	
	2955.8 ± 0.6[d]	CH_3 asym. stretching	0.251	
	2912.7 ± 0.4[d]	CH_3 asym. stretching	0.208	
	2864.1 ± 0.6[d]	CH_3 sym. stretching	0.023	
	2837.2 ± 0.1[d]	CH_3 sym. stretching	0.136	
	2536.0 ± 9.6[d]	OD stretching	0.263	
	2500.6 ± 1.5[d]	OD stretching	0.179	
	2430.6 ± 0.6[d]	OD stretching	1.260	
	2405.9 ± 5.0[d]	OD stretching	1.042	
	2199.6 ± 14.4[d]	CH_3 rocking + OD bending?	0.060	
	2174.4 ± 3.0[d]	CH_3 rocking + OD bending	0.034	
	1513.4 ± 0.1[d]	?	0.007	
	1477.8 ± 0.3[d]	CH_3 asym. bending	0.041	
	1463.5 ± 0.3[d]	CH_3 asym. bending	0.057	
	1235.8 ± 0.5	CH_3 rocking	0.038	
	1162.0 ± 2.0	CH_3 rocking	0.008	
	1124.0 ± 3.0	CH_3 rocking	0.005	
	1043.5 ± 0.1	CO stretching	0.797	
	966.3 ± 1.3[d]	OD bending	0.025	
	941.5 ± 0.9[d]	OD bending	0.067	
CD_3OD	2527.3 ± 3.3[d]	OD stretching	0.228	
	2451.6 ± 2.2[d]	OD stretching	0.918	
	2421.3 ± 2.5[d]	OD stretching	1.502	
	2244.7 ± 0.8[d]	CD_3 asym. stretching	0.134	
	2218.7 ± 0.4[d]	CD_3 asym. stretching	0.073	
	2202.8 ± 4.8[d]	CD_3 asym. stretching	0.105	
	2155.0 ± 2.5[d]	CD_3 asym. stretching	0.136	
	2073.0 ± 0.1[d]	CD_3 sym. stretching	0.190	
	1934.0 ± 5.0[d]	CO stretching	0.055	
	1127.5 ± 0.1[d]	CD_3 sym. stretching	0.180	
	1107.2 ± 0.8[d]	CD_3 asym. stretching	0.268	
	1064.4 ± 0.2[d]	CD_3 asym. stretching	0.077	
	981.5 ± 0.1	CO stretching	0.400	
	900.0 ± 0.5	CD_3 rocking	0.021	

[a] Values are in 3 monolayer. Bands at 1700−1600 cm^{-1} in CH_3OH, CH_2DOH, and CH_3OD are noise. [b] Bands were assigned on the basis of literature values.[26−29] [c] Values are normalized to the CO streching mode in CH_3OH at 1043.6 cm^{-1}. [d] Band positions and integrated area absorbance (relative integrated band strength) were obtained by the least-square method (peak deconvolution).

inefficient. Therefore, the maxima mentioned above are not due to desorption from the solid sample but are due to the successive H−D substitution reaction 4.

It can be seen that the decrease in CH_3OH was saturated at approximately −0.1 after the long exposure time. This saturation probably resulted from a chemical equilibrium and/or a slow diffusion rate of D atoms to the inside of the solid sample. To examine the former possibility, we performed an experiment in which solid CH_2DOH was exposed to cold D atoms at 10 K (see section 3.2 for details). No CH_3OH was observed, indicating that the unknown backward process $CH_2DOH \rightarrow CH_3OH$ does not proceed. Thus, the origin of saturation must be the latter; it seems that CH_3OH molecules at the surface of the solid sample easily react with D atoms, but buried CH_3OH molecules hardly react because of the very slow diffusion rate of D atoms into the bulk.

To investigate the influence of the translational temperature of the D atoms on reactivity, we performed the same experiment using D atoms at 50, 200, and 300 K. The results of these experiments are consistent with each other, suggesting that reaction 4 proceeds not via the Eley−Rideal (ER) process but via the Langmuir−Hinshelwood (LH) process: the surface reaction between adsorbed atoms and molecules on a surface. If the ER process is dominant in reaction 4, the reaction rate should become large with an increase in the translational temperature of D, because the ER process is a direct reaction between atoms impinging from the gas phase and adsorbed molecules on the surface. To confirm this scenario, we exposed solid CH_3OH to cold (100 K) D atoms at 30 K. Reaction 4 was not observed in this experiment within a duration of more than 180 min. This is due to a drop in the sticking coefficient of the D atom to the sample surface above ∼20 K,[5,7] and supports the dominance of the LH process in reaction 4.

The possible mechanisms of the H−D substitution reaction 4 are as follows:

$$CH_3OH + D \rightarrow CH_2OH + HD$$

$$CH_2OH + D \rightarrow CH_2DOH$$
$$CH_2DOH + D \rightarrow CHDOH + HD$$
$$CHDOH + D \rightarrow CHD_2OH \quad (A)$$
$$CHD_2OH + D \rightarrow CD_2OH + HD$$
$$CD_2OH + D \rightarrow CD_3OH$$

and

$$CH_3OH + D \rightarrow CH_3DOH^* \rightarrow CH_2DOH + H$$
$$CH_2DOH + D \rightarrow CH_2D_2OH^* \rightarrow CHD_2OH + H \quad (B)$$
$$CHD_2OH + D \rightarrow CHD_3OH^* \rightarrow CD_3OH + H$$

Process A consists of the repetition of the hydroxymethyl radical formation by H abstraction from the methyl side in methanol and the subsequent D addition to the radical to form methanol isotopologues; process B consists of the formation of excited intermediates such as CH_3DOH^* by D addition and the subsequent H−D exchange in the methyl group. Since the difference between A and B is in the formation of hydroxymethyl radicals, the detection of such radicals enables us to determine which process dominates the H−D substitution reaction. However, although hydroxymethyl radicals were not detected in this experiment, we cannot conclude that process B is the dominant process in the H−D substitution reaction. Even when these radicals are produced in process A, they will be consumed immediately by the reaction with D atoms because of the very fast rate of the radical atom reaction. Therefore, the average surface density of the radicals will be too low for detection, similar to the nondetection of HCO and CH_3O radicals in the experiment on successive hydrogenation of CO.[5] We detected particles of mass 3 (HD) and 1 (H) by QMS during the exposure. However, the atomic beam used in the present

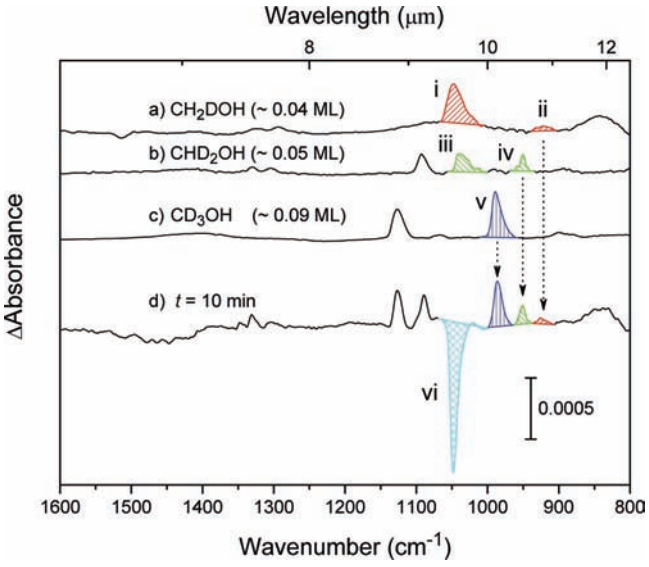

Figure 7. Example of band assignment in the spectrum obtained after D exposure. Spectra a, b, and c represent pure amorphous solid samples of CH_2DOH (0.04 ML), CHD_2OH (0.05 ML), and CD_3OH (0.09 ML) at 10 K, respectively, corresponding to the increase of these isotopologues in the solid CH_3OH sample exposed to D atoms for 10 min (d).

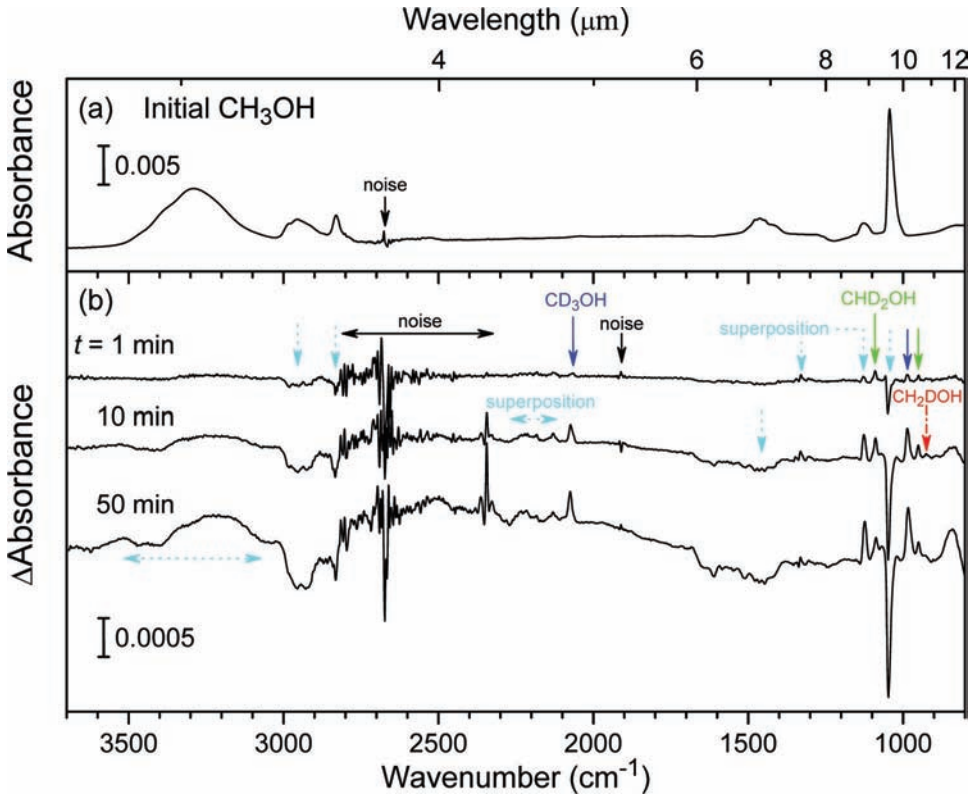

Figure 6. (a) Infrared absorption spectrum of initial (pre-exposure) amorphous solid CH_3OH (3 ML) deposited onto the Al substrate at 10 K. Absorbance is obtained as common logarithms. (b) Change in the spectrum after D exposure of 1, 10, and 50 min at 10 K. Spectra were obtained by subtracting the initial spectrum from D-exposed spectra. Peaks below and above the baseline represent decreases and increases, respectively, compared to the initial spectrum. Red (dashed-dotted), green (continuous), and blue (continuous) arrows represent increases in CH_2DOH, CHD_2OH, and CD_3OH, respectively. Sky-blue (dotted) arrows are a superposition of CH_3OH decreases and increases in isotopologues. Noise, mainly caused by the vibration of the He refrigerator, is denoted by black (continuous) arrows.

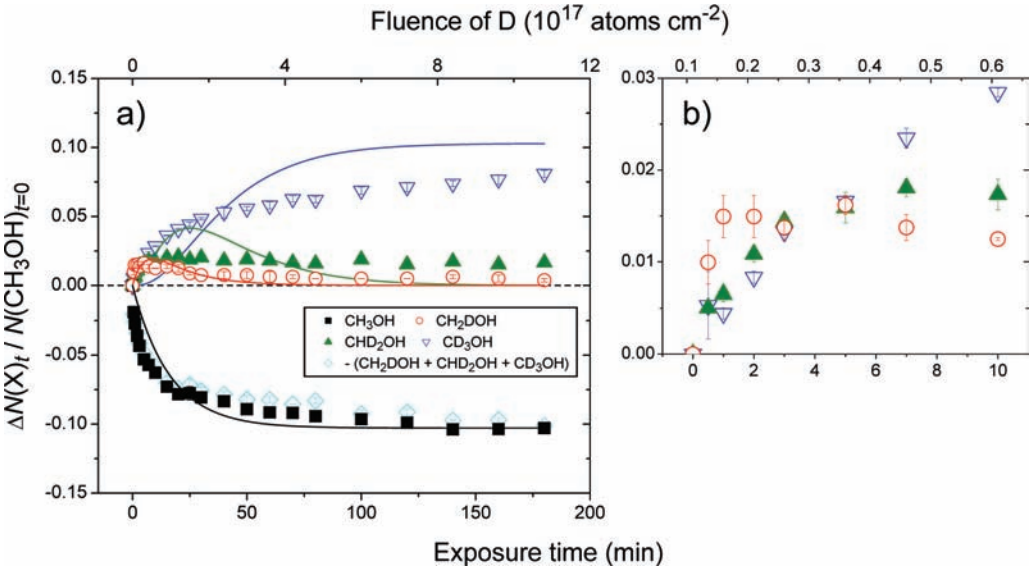

Figure 8. (a) Variation in column densities normalized to initial CH_3OH in the experiment in which amorphous solid CH_3OH (3 ML) was exposed to D atoms at 10 K. The upper abscissa represents the fluence of D atoms. The lines are the results of fitting using eq 8a−d. Error bars represent statistical error. The diamonds represent the sum of the products multiplied by −1. (b) Close-up of the products for exposure time of $t = 0-10$ min.

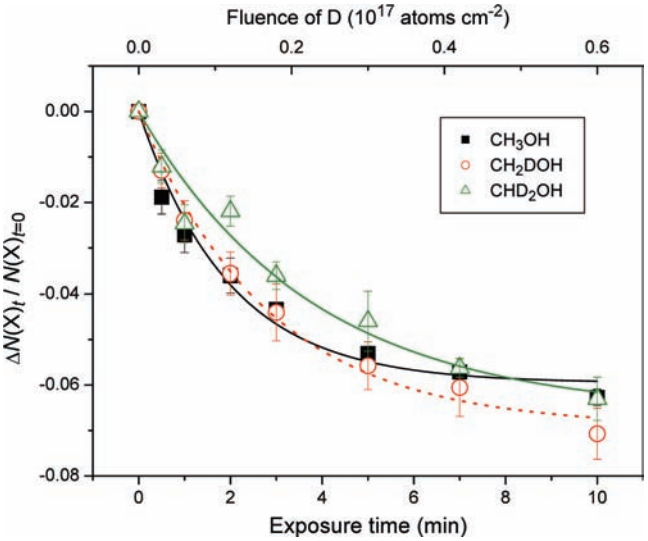

Figure 9. Decay of CH_3OH, CH_2DOH, and CHD_2OH in experiments in which amorphous solid CH_3OH, CH_2DOH, and CHD_2OH were exposed to D atoms at 10 K. The upper abscissa represents the fluence of D atoms. The lines are the results of fitting using single-exponential decay function (8a). Error bars represent statistical error.

experiment is a continuous beam, and thus the pressure during D exposure increases up to $\sim 2 \times 10^{-7}$ Torr. Therefore, it is unclear whether the origin of those masses is processes A and B or the background. As a result, it is difficult to evaluate the contribution of processes A and B to reaction 4 from the present experiment.

Isotopologues containing D in a hydroxyl group (e.g., CH_3OD) were not detected in the present experiment. This is due in part to the larger dissociation energy of the O−H bond ($CH_3OH \rightarrow CH_3O + H$) compared with the C−H bond ($CH_3OH \rightarrow CH_2OH + H$) in CH_3OH (by 4−11 kcal mol^{-1}).[21] In addition, the vibrationally adiabatic barrier heights of the following two channels for the reactions of CH_3OH with D atoms in the gas phase were calculated using an ab initio method:[22]

$$CH_3OH + D \rightarrow CH_2OH + HD \quad (5a)$$

$$\rightarrow CH_3O + HD \quad (5b)$$

The calculated barrier heights for reactions 5a,b are 7.72 and 12.2 kcal mol^{-1},[22] respectively, suggesting that H abstraction from the methyl group (5a) generally proceeds faster than from the hydroxyl group (5b).

Although the H−D exchange process (B) has never been reported on a solid surface, the gas-phase H−H exchange reaction was investigated by Osamura et al.[23] Using the ab initio method, they obtained the barrier height for H addition to the C side in CH_3OH and subsequent exchange for another H atom bonded with C ($CH_3OH + H' \rightarrow CH_3H'OH^* \rightarrow CH_2H'OH + H$) to be 40.4 kcal mol^{-1}, and thus they concluded that this H−H exchange reaction does not occur at low temperatures. Therefore, it is reasonable to consider that the H−D substitution reaction 4 proceeds via process A rather than process B. Considering the theoretically calculated barrier height of 7.72 kcal mol^{-1},[22] we find that the H-abstraction reaction is likely to proceed via a quantum mechanical tunneling reaction at a low-temperature surface.

We determined the effective rate constants for the H−D substitution reaction 4 from the experimental results on the assumption that the reaction is dominated by process A:

$$CH_3OH + D \xrightarrow{k_1'} CH_2OH + HD \quad (6a)$$

$$CH_2OH + D \xrightarrow{k_1''} CH_2DOH \quad (6b)$$

$$CH_2DOH + D \xrightarrow{k_2'} CHDOH + HD \quad (6c)$$

$$CHDOH + D \xrightarrow{k_2''} CHD_2OH \quad (6d)$$

$$CHD_2OH + D \xrightarrow{k_3'} CD_2OH + HD \quad (6e)$$

$$CD_2OH + D \xrightarrow{k_3''} CD_3OH \quad (6f)$$

where k_n' and k_n'' (cm^2 molecule^{-1} s^{-1}, $n = 1-3$) are the reaction rate constants. Since the rate constants k_n' for hydroxymethyl radicals CH_2OH, CHDOH, and CD_2OH must be much smaller than those for D-addition k_n'' ($n = 1-3$), the rate-

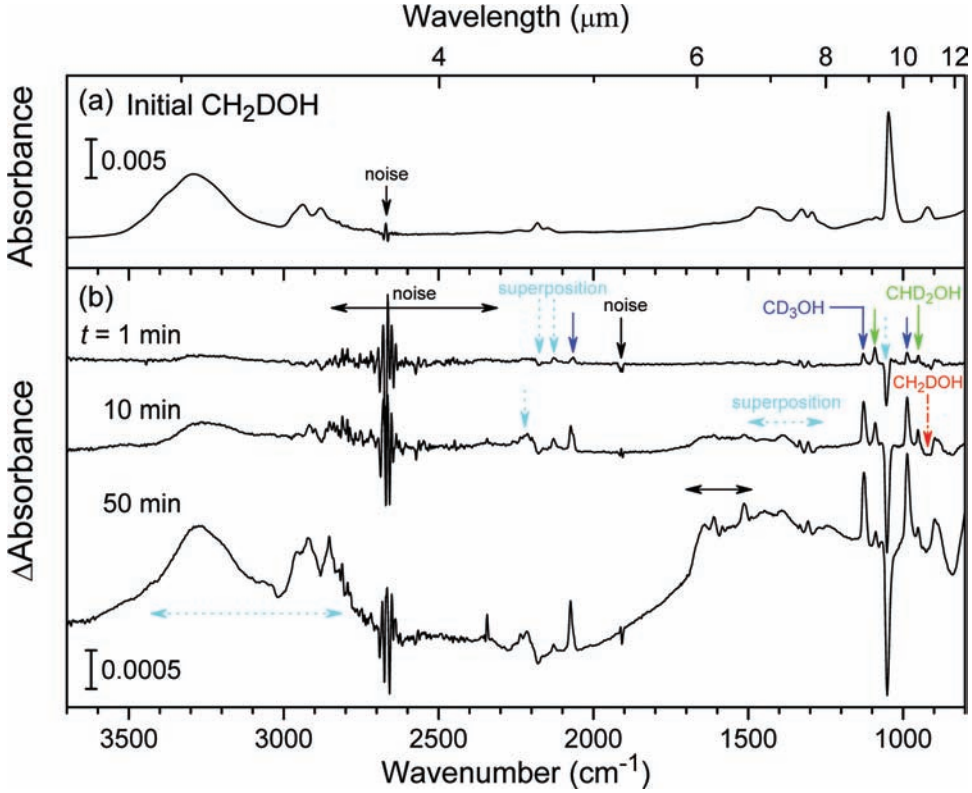

Figure 10. (a) Infrared absorption spectrum of initial (pre-exposure) amorphous solid CH_2DOH deposited at 10 K. (b) Spectral change after D exposure for 1, 10, and 50 min at 10 K. Absorbance was obtained as common logarithms. The spectra were obtained by subtracting the initial spectrum from D-exposed spectra. Red (dashed-dotted), green (continuous), and blue (continuous) arrows show a decrease in CH_2DOH, increases in CHD_2OH and CD_3OH. Sky-blue (dotted) arrows show a superposition of CH_2DOH decreases and increases in the other isotopologues. Noise, mainly caused by the vibration of the He refrigerator, is denoted by black (continuous) arrows.

TABLE 2: Effective Rate Constants for the H-Abstraction Reaction by D Atoms at 10 K

n	pseudo-first order: $k_n'N_D$[a] (10^{-3} s^{-1})	second order: $k_n'P^{1/2}$[b] (10^{-11} cm^2 molecule^{-1} s^{-1})
1	8.5 ± 1.1	1.6 ± 0.21
2	5.9 ± 0.57	1.1 ± 0.11
3	4.4 ± 1.0	0.82 ± 0.19

[a] Fitting results for decay of sample molecule in each experiment. [b] Effective rate constants calculated using $N_D = 53.9(1 \times 10^{14}P)^{1/2}$.

determining steps for the H−D substitution reaction 4 are 6a,c,e. Hence, the rate constants k_1', k_2', and k_3' can be approximated as k_1, k_2, and k_3, respectively. Finally, the rate equations for reaction 4 are expressed as follows:

$$\frac{dN(CH_3OH)_t}{dt} = -k_1'N_D N(CH_3OH)_t \quad (7a)$$

$$\frac{dN(CH_2DOH)_t}{dt} = k_1'N_D N(CH_3OH)_t - k_2'N_D N(CH_2DOH)_t \quad (7b)$$

$$\frac{dN(CHD_2OH)_t}{dt} = k_2'N_D N(CH_2DOH)_t - k_3'N_D N(CHD_2OH)_t \quad (7c)$$

$$\frac{dN(CD_3OH)_t}{dt} = k_3'N_D N(CHD_2OH)_t \quad (7d)$$

where $N(X)_t$ (molecule cm^{-2}) is the column density at t, and N_D is the surface density of D atoms (molecule cm^{-2}). The solution of 7a−d under the initial condition ($t = 0$) of $N(CH_2DOH)_0 = N(CHD_2OH)_0 = N(CD_3OH)_0 = 0$ is given by

$$\frac{N(CH_3OH)_t}{N(CH_3OH)_0} = e^{-k_1'N_D t} \quad (8a)$$

$$\frac{N(CH_2DOH)_t}{N(CH_3OH)_0} = \frac{k_1'}{k_2' - k_1'}(e^{-k_1'N_D t} - e^{-k_2'N_D t}) \quad (8b)$$

$$\frac{N(CHD_2OH)_t}{N(CH_3OH)_0} = \frac{k_1'k_2'}{k_2' - k_1'}\left(\frac{e^{-k_1'N_D t} - e^{-k_3'N_D t}}{k_3' - k_1'} - \frac{e^{-k_2'N_D t} - e^{-k_3'N_D t}}{k_3' - k_2'}\right) \quad (8c)$$

$$\frac{N(CD_3OH)_t}{N(CH_3OH)_0} = \frac{k_1'k_2'k_3'}{k_2' - k_1'}\left[\frac{e^{-k_1'N_D t} - 1}{-k_1'(k_3' - k_1')} - \frac{e^{-k_3'N_D t} - 1}{-k_3'(k_3' - k_1')} - \frac{e^{-k_2'N_D t} - 1}{-k_2'(k_3' - k_2')} + \frac{e^{-k_3'N_D t} - 1}{-k_3'(k_3' - k_2')}\right] \quad (8d)$$

where $N(CH_3OH)_0$ is the column density of CH_3OH at $t = 0$ (molecule cm^{-2}). The time variation of N_D is expressed as follows:[24]

$$\frac{dN_D}{dt} = Pf_D - k_{D-D}N_D^2 - R_D N_D \quad (9)$$

where P is the sticking coefficient of the D atom, f_D is the flux of D atoms (molecule cm^{-2} s^{-1}), k_{D-D} is the rate constant for recombination of D atoms ($D + D \rightarrow D_2$) (cm^2 molecule^{-1} s^{-1}),

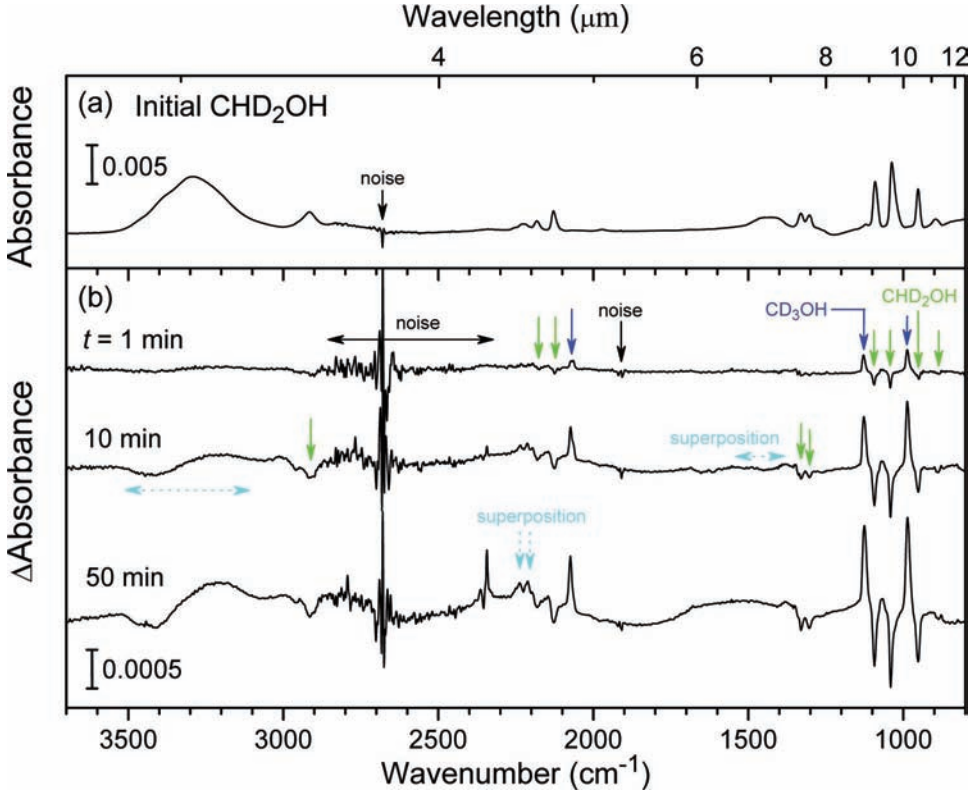

Figure 11. (a) Infrared absorption spectrum of initial (pre-exposure) amorphous solid CHD_2OH deposited at 10 K. (b) Spectral change after D exposure for 1, 10, and 50 min at 10 K. Spectra were obtained by subtracting the initial spectrum from the D-exposed spectra. Absorbance was obtained as common logarithms. Green (continuous) and blue (continuous) arrows show a decrease in CHD_2OH and an increase in CD_3OH. Sky-blue (dotted) arrows show a superposition of CHD_2OH decreases and increases in CD_3OH. Noise, mainly caused by the vibration of the He refrigerator, is denoted by black (continuous) arrows.

and R_D is the rate constant for desorption of D atoms (molecule s^{-1}). In the right-hand side of eq 9, the terms for D loss by reaction with CH_3OH, CH_2DOH, and CHD_2OH are neglected, because these reactions are very slow compared with recombination and desorption. The calculation by Chigai et al. demonstrates that N_D immediately becomes $N_D = 53.9 \times (f_D P)^{1/2}$ at the beginning ($t < 10^{-9}$ s) of D exposure and stays constant during exposure under the present experimental conditions.

The solid lines in Figure 8 show the results of fitting by the least-square method using 8a−d. None of the fitted curves reproduce the experimental data well. The crucial difference between the fitted curves and the experimental data can be seen in CH_2DOH and CHD_2OH; these curves approach zero beyond their maxima, while the experimental data for CH_2DOH and CHD_2OH are almost constant after ∼50 min and do not approach zero within the duration of the experiment. This difference may be attributable to the slow diffusion rate of D atoms to the inside of the solid samples, as mentioned above; molecules at the surface of the solid sample easily react with D atoms, but buried molecules react with more difficulty and tend to remain intact. Therefore, we fit the decay of CH_3OH at a duration of $t = 0-10$ min using eq 8a alone (black line in Figure 9). The fitted curve reproduces the decay of CH_3OH well. The obtained pseudo-first-order reaction rate for reaction 6a is $(8.5 \pm 1.1) \times 10^{-3}$ s^{-1}. Assuming that $N_D = 53.9(1 \times 10^{14}P)^{1/2}$, the effective second-order rate constant can be obtained as a function of the sticking coefficient of D atoms: $k_1'P^{1/2} = (1.6 \pm 0.21) \times 10^{-11}$ cm^2 $molecule^{-1}$ s^{-1}.

3.2. Exposure of Amorphous Solid CH_2DOH and CHD_2OH to D Atoms. To obtain k_2' and k_3', respectively, we exposed solid CH_2DOH and CHD_2OH at 10 K to cold D atoms. The experimental procedure and conditions were the same as those for solid CH_3OH. The thickness of the samples was also the same as in the CH_3OH + D experiment. Figures 10 and 11 show the infrared absorption spectra of solid CH_2DOH and CHD_2OH before exposure and the change in the spectra after exposure to cold D atoms at 100 K, respectively. In the experiment using CH_2DOH, the formation of CHD_2OH and CD_3OH is observed with the consumption of CH_2DOH (Figure

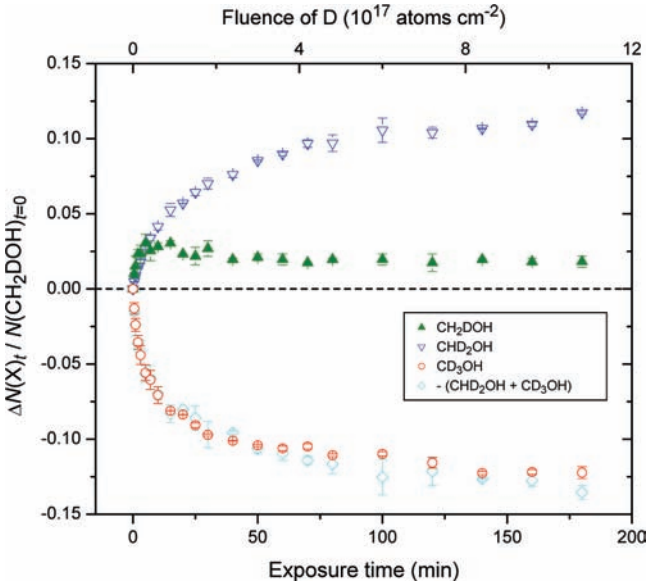

Figure 12. (a) Variation in column densities normalized to initial CH_2DOH in the experiment in which amorphous solid CH_2DOH (3 ML) was exposed to D atoms at 10 K. The upper abscissa represents the fluence of D atoms. The error bars represent statistical error. Diamonds represent the sum of the products multiplied by −1.

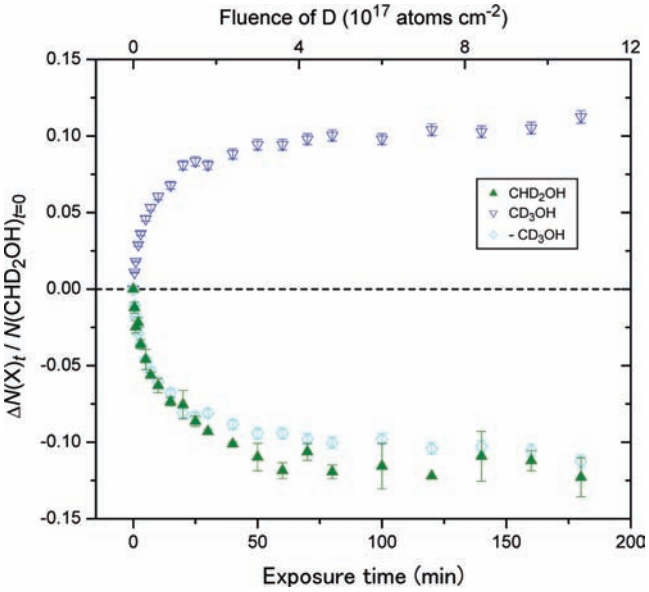

Figure 13. (a) Variation in column densities normalized to initial CHD_2OH in the experiment in which amorphous solid CHD_2OH (3 ML) was exposed to D atoms at 10 K. The upper abscissa represents the fluence of D atoms. The error bars represent statistical error. Diamonds represent CD_3OH multiplied by −1.

TABLE 3: Relative Rates for H-Abstraction Reaction by D Atoms at 10 K

	relative rates[a]	calculation[b]
k_2'/k_1'	0.69 ± 0.11	0.576
k_3'/k_1'	0.52 ± 0.14	
k_3'/k_2'	0.75 ± 0.18	

[a] Obtained from the pseudo-first-order rates in Table 2. [b] Ab initio calculation by Lendvay et al.[25]

10b); in the experiment using CHD_2OH, the only product is CD_3OH (Figure 11b). The backward process (e.g., $CH_2DOH \rightarrow CH_3OH$) and other products (HDCO, D_2CO, etc.) are not observed at all. Variations in the column densities of the samples due to D atom exposure are shown in Figures 12 and 13. H−D substitution reactions were found to proceed as follows in each experiment:

$$CH_2DOH \rightarrow CHD_2OH \rightarrow CD_3OH$$

and

$$CHD_2OH \rightarrow CD_3OH$$

For the reasons described in section 3.1, we fit the data of CH_2DOH and CHD_2OH decay to single-exponential decay (8a, Figure 9). The obtained pseudo-first-order rate and effective second-order rate constants are summarized in Table 2.

Assuming that P, k_{D-D}, and R_D are independent of the initial solid sample types, the relationships between the rate constants k_n' ($n = 1-3$) were found to be $k_1' > k_2' > k_3'$; the ratios $k_2'/k_1' = 0.69 \pm 0.11$ and $k_3'/k_1' = 0.52 \pm 0.14$ were obtained from the results of fitting for CH_3OH, CH_2DOH, and CHD_2OH samples (Table 3). This relationship is mainly due to the difference in activation energy for the H-abstraction reaction 6a,c,e (i.e., the secondary kinetic isotope effect). Using ab initio methods, Lendvay et al. calculated the secondary kinetic isotope effect for the reactions $CH_3OH + H \rightarrow CH_2OH + H_2$ and $CH_2DOH + H \rightarrow CHDOH + H_2$ at 300−2000 K (ref 25) and reported a k_2'/k_1' ratio of 0.576 at 300 K. This value is smaller than the experimentally obtained ratio of 0.69 ± 0.11. Although the origin of the difference between the theory and our experiments is unclear, it may have arisen from differences in conditions such as reactants (H atom vs D atom), phase (gas vs solid), and temperature (300 K vs 10 K).

3.3. Exposure of Amorphous Solid CH_3OD to D Atoms. An experiment in which amorphous solid CH_3OD with a thickness of 3 monolayer was exposed to D atoms at 10 K was also carried out. Although the resulting changes in the IR spectrum are not shown here, we observed a decrease in CH_3OD and the appearance of deuterated molecules such as CD_3OD. However, kinetic data could not be obtained for this experiment because the integrated band strengths of CH_2DOD and CHD_2OD are unknown. The bands of CH_2DOD and CHD_2OD partially overlap with those of CH_3OD, and thus we could not quantify either the decrease in CH_3OD or the yields of CH_2DOD, CHD_2OD, and CD_3OD.

3.4. Exposure of Amorphous Solid CD_3OD to D Atoms. We also exposed amorphous solid CD_3OD (3 ML) to D atoms at 10 K over a period of 180 min, but no change was observed in the IR spectra (data not shown). This result indicates that the D-abstraction reaction by D atoms ($CD_3OD + D \rightarrow CD_2OD + D_2$) is inhibited or alternatively that the D-abstraction reaction does proceed within the experimental duration, but the resulting CD_2OD radicals immediately react with D atoms to form CD_3OD. It is not currently clear whether the D-abstraction reaction actually proceeds on a solid surface at 10 K.

4. Conclusion

We performed experiments in which solid CH_3OH, CH_2DOH, and CHD_2OH at 10 K were exposed to cold D atoms at 100 K. The H−D substitution reactions $CH_3OH \rightarrow CH_2DOH \rightarrow CHD_2OH \rightarrow CD_3OH$ were observed; these reactions are likely to proceed via quantum mechanical tunneling. The effective reaction rate constants for the H−D substitution reaction were estimated, and the secondary kinetic isotope effects for the reaction steps were derived: values of 0.69 ± 0.11 and 0.52 ± 0.14 were obtained for the second and the third step, respectively, compared with the first step.

Acknowledgment. We would like to thank Dr. H. Hidaka and Dr. T. Chigai for helpful discussions, and Mr. K. Shinbori, Mr. S. Nakatsubo, and Mr. K. Fujita for making several components of the ASURA system. A.N. is supported by the Japan Society for the Promotion of Science via a JSPS Research Fellowship for Young Scientists. This research was supported in part by a Grant-in-Aid for Scientific Research from the Ministry of Education, Culture, Sports, Science and Technology of Japan and the Japan Society for the Promotion of Science.

References and Notes

(1) Goldanskii, V. I. *Nature* **1979**, *279*, 109.
(2) Herbst, E.; Chang, Q.; Cuppen, H. M. *J. Phys.: Conf. Ser.* **2005**, *6*, 18.
(3) Watanabe, N.; Kouchi, A. *Astrophys. J.* **2002**, *571*, L173.
(4) Watanabe, N.; Shiraki, T.; Kouchi, A. *Astrophys. J.* **2003**, *588*, L121.
(5) Watanabe, N.; Nagaoka, A.; Shiraki, T.; Kouchi, A. *Astrophys. J.* **2004**, *616*, 638.
(6) Hidaka, H.; Watanabe, N.; Shiraki, T.; Nagaoka, A.; Kouchi, A. *Astrophys. J.* **2004**, *614*, 1124.
(7) Watanabe, N.; Nagaoka, A.; Hidaka, H.; Shiraki, T.; Chigai, T.; Kouchi, A. *Planet. Space Sci.* **2006**, *54*, 1107.
(8) Hidaka, H.; Kouchi, A.; Watanabe, N. **2006**, submitted to *J. Chem. Phys.*
(9) Nagaoka, A.; Watanabe, N.; Kouchi, A. *Astrophys. J.* **2005**, *624*, L29.

(10) Nagaoka, A.; Watanabe, N.; Kouchi, A. *ASTROCHEMISTRY: From Laboratory Studies to Astronomical Observations;* AIP Conference Proceedings, **2006**, *855*, 69.
(11) For example, see Hudson, R. L.; Shiotani, M.; Williams *Chem. Phys. Lett*. **1977**, *48*, 193.
(12) Hiraoka, K.; Wada, A.; Kitagawa, H.; Kamo, M.; Unagiike, H.; Ueno, T. *Astrophys. J.* **2005**, *620*, 542.
(13) Moore, M. H.; Ferrante, R. F.; Hudson, R. L.; Nuth, J. A., III; Donn, B. *Astrophys. J.* **1994**, *428*, L81.
(14) McCullough, R. W.; Geddes, J.; Donnelly, A.; Liehr, M.; Hughes, M. P.; Gilbody, H. B. *Meas. Sci. Technol.* **1993**, *4*, 79.
(15) Walraven, J. T. M.; Silvera, I. F. *Rev. Sci. Instrum.* **1982**, *53*, 1167.
(16) *CRC Handbook of Chemistry and Physics*, 63rd ed.; Weast, R. C., Ed.; CRC Press: Boca Raton, FL, 1982.
(17) d'Hendecourt, L. B.; Allamandola, L. J. *Astron. Astrophys., Suppl. Ser.* **1986**, *64*, 453.
(18) Hudgins, D. M.; Sandford, S. A.; Allamandola, L. J.; Tielens, A. G. G. M. *Astron. Astrophys., Suppl. Ser.* **1993**, *86*, 713.
(19) After deposition, we measured the TPD spectrum for the molecules desorbing from the substrate using QMS. The heating rate of the substrate was 2 K min^{-1}. The total number of molecules in the sample can be obtained by integrating the TPD spectrum. As a result, the thicknesses of the samples were found to be approximately 6 and 12 monolayer for deposition times of 10 and 20 min, respectively.
(20) An experiment in which the substrate, without the solid sample, at 10 K was exposed to D atoms at 100 K for several hours.
(21) Bauschlicher, C. W.; Langhoff, S. R., Jr.; Walch, S. P. *J. Chem. Phys.* **1992**, *96*, 450.
(22) Kerkeni, B.; Clary, D. C. *J. Phys. Chem. A* **2004**, *108*, 8966.
(23) Osamura, Y.; Roberts, H.; Herbst, E. *Astron. Astrophys.* **2004**, *421*, 1101.
(24) Chigai, T. et al. In preparation.
(25) Lendvay, G.; Berces, T.; Marta, F. *J. Phys. Chem. A* **1997**, *101*, 1588.
(26) Falk, M.; Whalley, E. *J. Chem. Phys*. **1961**, *34*, 1554.
(27) Serrallach, A.; Meyer, R.; Gunthard, Hs. H. *J. Mol. Spectrosc.* **1974**, *52*, 94.
(28) Huberty, J. S.; Madix, R. J. *Surf. Sci*. **1996**, *360*, 144.
(29) Barros, R. B.; Garcia, A. R.; Ilharco, L. M. *Chem. Phys. Chem*. **2005**, *6*, 1299.